FEBS Letters 495 (2001) 126–130 FEBS 24805

Increase in the molecular weight and radius of gyration of apocalmodulin induced by binding of target peptide: evidence for complex formation

Yoshinobu Izumi[a,*], Shigeo Kuwamoto[a], Yuji Jinbo[a], Hidenori Yoshino[b]

[a] *Graduate Program of Human Sensing and Functional Sensor Engineering, Graduate School of Science and Engineering, Yamagata University, 4-3-16 Jo-nan, Yonezawa 992-8510, Japan*

[b] *Department of Chemistry, Sapporo Medical University, S-1, W-17, Chuo-ku, Sapporo 060-0061, Japan*

Received 6 November 2000; revised 12 March 2001; accepted 26 March 2001

First published online 6 April 2001

Edited by Hans Eklund

Abstract Small-angle X-ray scattering was used to investigate a complex state of apocalmodulin induced by the binding of a Ca^{2+}/calmodulin-dependent protein kinase IV calmodulin target site. Upon binding of the peptide, the molecular weight for apocalmodulin increased by 8.4%, which provides direct evidence for the formation of a calmodulin/target peptide complex. Comparison of the radius of gyration and Kratky plots of the apocalmodulin/peptide complex with those of apocalmodulin indicates that the overall conformation remains unchanged but the flexibility of the central linker decreases. An analysis of residue pairs between calmodulin and the target peptides suggests that the complex formation is induced by electrostatic interactions and subsequent van der Waals interactions. © 2001 Published by Elsevier Science B.V. on behalf of the Federation of European Biochemical Societies.

Key words: Apocalmodulin; Ca^{2+}/calmodulin-dependent protein kinase IV calmodulin target site; Small-angle X-ray scattering; Complex state; Linker flexibility; Electrostatic interaction

1. Introduction

Calmodulin (CaM) is a ubiquitous Ca^{2+}-binding protein of 148 residues that regulates a variety of physiological processes in a Ca^{2+}-dependent manner [1]. The regulation is achieved through the interaction of Ca^{2+}-saturated CaM (Ca^{2+}/CaM) with a large number of target enzymes [2–4]. The Ca^{2+}/CaM molecule adopts a dumbbell-shaped structure in which the two lobes are connected by a highly flexible linker [5–11], while the structure of Ca^{2+}/CaM complexed with a peptide from target enzymes takes a compact globular shape caused by the bending of the central linker [12–17]. These structural studies suggest that the flexibility of the central linker and the two hydrophobic patches in Ca^{2+}/CaM play an important role in target recognition.

Although most published works were done in the presence of saturating Ca^{2+} concentrations, there are some target proteins, such as melittin, seminal plasmin [18], mastoparan [19,20], the CaM-binding domain of cyclic nucleotide phosphodiesterase (PDE1A2) [21] and smooth muscle myosin light chain kinase (smMLCK) RS20 [22], that significantly interacted also with Ca^{2+}-free CaM (apocalmodulin, apoCaM) or only with the apoCaM as neuromodulin [23]. Recently, it is presumed that apoCaM interacts with these peptides utilizing different binding motifs such as the IQ motif observed in neuromodulin. However, little is known about the mechanism of apoCaM's interaction with its target peptides and the overall conformation of apoCaM/peptide complexes. What is the physiological role of apoCaM/peptide complexes? It has been hypothesized that the apoCaM/RS20 complex is an intermediate in the formation of the Ca^{2+}/CaM/RS20 complex [24].

The aim of the present study is to investigate the complex state in apoCaM induced by the binding of a peptide with Ca^{2+}-dependent CaM-binding motifs by small-angle X-ray scattering (SAXS). We used a 19-residue peptide encompassing the Ca^{2+}/CaM-dependent protein kinase IV (human) CaM target site as a natural target-binding domain of CaM [25–27]. This peptide has been classified as a 1-5-8-14 motif [28]. The present results provide the first detailed SAXS evidence for the formation of apoCaM/peptide complex.

2. Materials and methods

2.1. Materials

A 19-residue peptide having the sequence RRKLKAAVKAVVASSRLGS corresponding to the CaM-binding domain (residues 323–341) of the Ca^{2+}/CaM-dependent protein kinase IV (human) (referred to as the CaMKIV-19 peptide) was synthesized on an Applied Biosystems Model 431A Peptide synthesizer using the general procedure and purified by reverse phase high-performance liquid chromatography. Bovine brain CaM was prepared and purified by the exact same methods as previously described [29].

2.2. SAXS measurements

The basic medium used for the SAXS measurements was 50 mM Tris–HCl, pH 7.6, and 120 mM NaCl. Ca^{2+}-free proteins were placed in 1 mM EDTA. The apoCaM/CaMKIV-19 peptide complex was prepared by mixing the protein with a 1.05-fold molar excess of the peptide. The protein concentrations were 7.5, 10.0, 12.5, 15.0, 17.5 and 20.0 mg/ml. The concentration of proteins was determined by the method of Lowry et al. [30].

The measurements were performed using synchrotron orbital radiation with an instrument for SAXS installed at BL-10C of Photon Factory, Tsukuba [31]. An X-ray wavelength of 1.488 Å was selected. The samples were contained in a mica cell with a volume of 70 μl, and the temperature was maintained at 25.0 ± 0.1°C by circulating water through the sample holder. The reciprocal parameter, s, equal to $2\sin\theta/\lambda$, was calibrated by the observation of a peak from dried chicken collagen, where 2θ is the scattering angle and λ is the X-ray wavelength. Scattering data were collected for 200 s at various protein concentrations.

Two methods of data analysis were used. The first method was that of Guinier [32]. The scattering intensity $I(s, c)$ measured as a function of s at a finite protein concentration, c, is given by:

$$I(s, c) = I(0, c)\exp\{-(4\pi^2/3)R_g(c)^2 s^2\} \quad (1)$$

*Corresponding author. Fax: (81)-238-26 3177.
E-mail: yizumi@dip.yz.yamagata-u.ac.jp

0014-5793/01/$20.00 © 2001 Published by Elsevier Science B.V. on behalf of the Federation of European Biochemical Societies.
PII: S0014-5793(01)02375-4

where $I(0, c)$ is the scattering intensity at $s=0$ and $R_g(c)$ is the radius of gyration at a concentration, c. In the dilute limit, $I(0, c)$ is given by:

$$Kc/I(0, c) = 1/M + 2A_2c + \ldots \quad (2)$$

where K is a constant, M is the molecular weight of the protein, and A_2 is the second virial coefficient. In the dilute limit, R_g is given by:

$$R_g^2 = R_0^2 - B_{if}c + \ldots \quad (3)$$

where R_0 is the radius of gyration at infinite dilution and B_{if} is the parameter of interparticle interference [33]. Using Eqs. 2 and 3, we estimated the four parameters M, A_2, R_0 and B_{if}. For the analysis, the range of s (Å^{-1}) was 4.4×10^{-3} to 1.24×10^{-2} for all samples measured. The second method was that of Kratky [34], which is defined by the plot of $s^2I(s, 0)$ versus s (the Kratky plot). The Kratky plot provides the structural characteristics (e.g. molecular shape) of a chain polymer [34–37] and a biopolymer [38]. For the analysis, all data to $s=0.06$ Å^{-1} were used.

3. Results

3.1. Guinier region of the scattering profile

Examples of Guinier plots ($\ln I(s)$ versus s^2) for apoCaM in the absence and presence of target peptide over the concentration series are shown in Fig. 1. In all of the samples studied here, there is no evidence of any upward curvature at low s values in the Guinier plots, which indicates that the data are free from the aggregation of samples. The values of $Kc/I(0, c)$ evaluated from the intercepts of the Guinier plots are shown as a function of protein concentration in Fig. 2. Plots in Fig. 2 are also linear over the entire concentration range, and the values of $[Kc/I(0, c)]_{c=0}$ extrapolated to infinite dilution for apoCaM in the absence and presence of target peptide have the inverse molecular weight appropriate for the soluble monomer. The molecular weights M and the second virial coefficients A_2 were calculated using Eq. 2 and compiled in Table 1. The value of M increased about 8.4% in the presence of 1 mol of the target peptide, whose increment almost corresponds to the molecular weight of 1 mol of the target peptide (about 11.9%), while the value of A_2 decreased about 30%. The increase in the molecular weight provides the direct evidence that a complex is formed between apoCaM and the target peptide even in the absence of Ca^{2+}.

Radii of gyration at finite concentrations were calculated from the slopes of the Guinier plots using Eq. 1 and are shown as a function of protein concentration in Fig. 3. The linear increase with decreasing protein concentration was observed. The slopes of these lines, which arise from interparticle interference effects, represent a virial coefficient [32].

Table 1 compiles the values of R_0 and B_{if}. The formation of a complex with the target peptide increases the radius of gyration of apoCaM by 1.0 ± 0.3 Å in comparison with that in the absence of target peptide. Furthermore, the formation of the complex decreases the value of B_{if} by 16%.

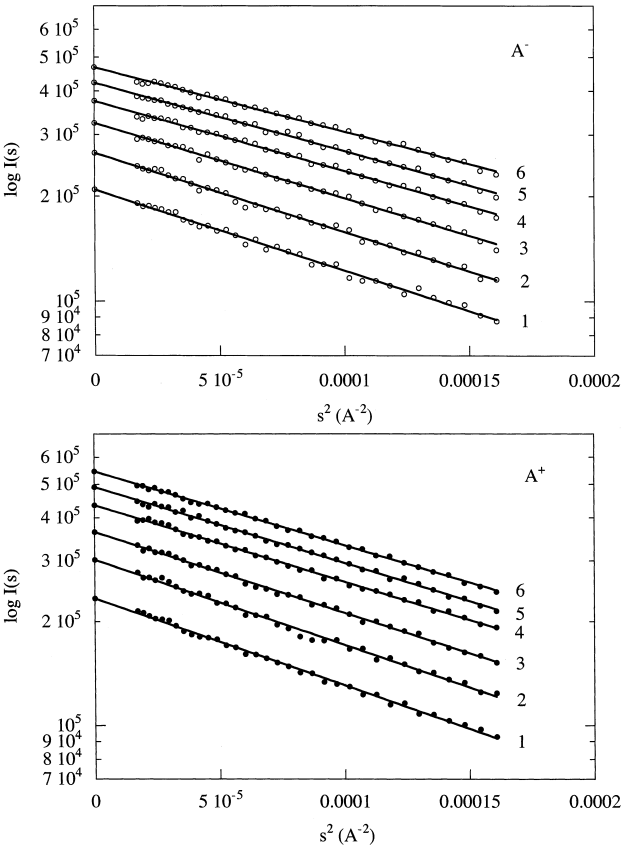

Fig. 1. Guinier plots for apoCaM (A^-) and apoCaM/CaMKIV-19 peptide complex (A^+) at various protein concentrations: (1) 7.5 mg/ml; (2) 10.0 mg/ml; (3) 12.5 mg/ml; (4) 15.0 mg/ml; (5) 17.5 mg/ml; (6) 20.0 mg/ml.

3.2. Kratky region of the scattering profile

Fig. 4 shows the Kratky plots for apoCaM in the absence and presence of target peptide. The Kratky plot for apoCaM without the target peptide is characterized by the presence of a broad asymmetric maximum near $s=0.0153$ Å^{-1}, indicating that apoCaM without peptide adopts a dumbbell-shaped structure. In the presence of target peptide, the changes in the Kratky plot are very slight, i.e. the position of the maximum shifts to the low value of $s=0.0139$ Å^{-1}. The results indicate that the overall size of the complex increases but apoCaM still preserves a dumbbell-shaped structure even in the presence of target peptide.

4. Discussion

4.1. Solution structure of apoCaM/CaMKIV-19 peptide complex

The SAXS analysis shows that the values of M and R_0

Table 1
Molecular weight (M) and second virial coefficient (A_2), radius of gyration at infinite dilution (R_0), parameter of interparticle interference (B_{if}) and center-to-center distance between two lobes (L) for CaM at pH 7.6

	$10^{-3}M$	10^4A_2 (mol cm^3/g^2)	R_0 (Å)	$10^{13}B_{if}$ (cm^5/g)	L[a] (Å)
ApoCaM	16.7 ± 0.8	3.1 ± 0.3	21.2 ± 0.3	6.8 ± 0.6	33.2 ± 0.8
ApoCaM/CaMKIV-19 peptide	18.1 ± 0.9	1.9 ± 0.2	22.2 ± 0.3	5.7 ± 0.5	35.7 ± 0.8
$4Ca^{2+}$/CaM [12,52]	16.7 ± 0.8	2.1 ± 0.2	21.5 ± 0.3	4.7 ± 0.4	33.9 ± 0.8

[a] $R_d = 13.2$ Å was assumed [33].

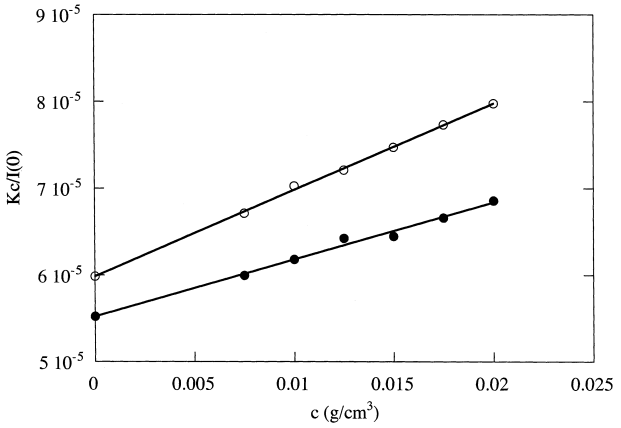

Fig. 2. Zimm plots for apoCaM (○) and apoCaM/CaMKIV-19 peptide complex (●).

increase, while A_2 and B_{if} decrease, upon binding of 1 mol of the target peptide. The most straightforward interpretation for the increase of M and R_0 is that a complex is created between apoCaM and CaMKIV-19 peptide upon binding of 1 mol of the peptide. The results for the Kratky plots indicate that apoCaM with the peptide essentially adopts a dumbbell-shaped structure similar to that without peptide, although its overall size becomes larger than that of the apoCaM without peptide.

Based on the dumbbell-shaped structure, the center-to-center distance between two lobes, L, is given by:

$$L = 2\sqrt{R_0^2 - R_d^2} \quad (4)$$

[39], where R_d is the radius of gyration of each lobe. We used the experimental value of $R_d = 13.2 \pm 0.2$ Å for the F34 fragment in the Ca^{2+}-free form [33]. Using R_0 in Table 1, the values of L calculated for apoCaM were compiled in Table 1. The 1 Å increase in R_0, induced by binding of 1 mol of the target peptide, corresponds to the 2.5 Å increase in L. The increase in L is consistent with the shift of the peak from 0.0153 to 0.0139 $Å^{-1}$ in the Kratky plots. What is the meaning of the increase in L? As reported previously [40–42], the two lobes in apoCaM tumble independently in solution and the Ca^{2+}-binding loops (residues 20–31, 56–67, 93–104 and

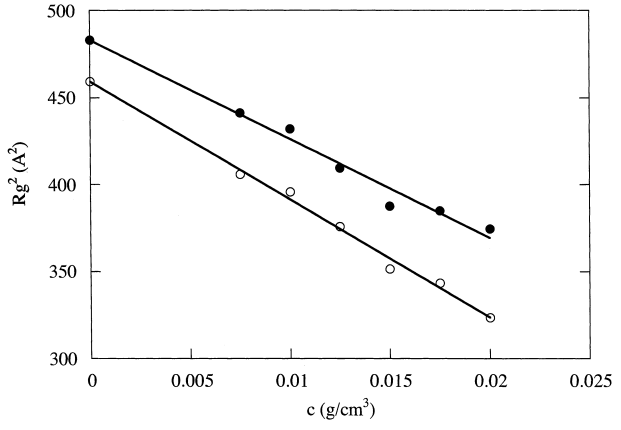

Fig. 3. The square of the radius of gyration, R_g^2, for apoCaM (○) and apoCaM/CaMKIV-19 peptide complex (●) as a function of the protein concentration.

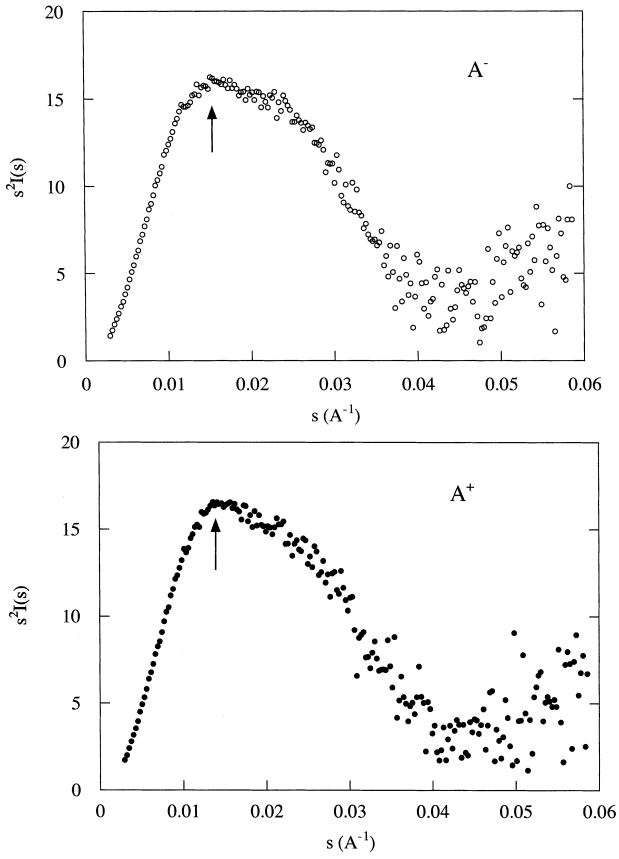

Fig. 4. Kratky plots for apoCaM (A^-) and apoCaM/CaMKIV-19 peptide complex (A^+).

129–140) are partially unstructured. The increase in R_0 induced upon binding of Ca^{2+} is rather small as shown in Table 1, although it leads to a drastic decrease in the loop flexibility. It is thought that in the absence of Ca^{2+}, the loop flexibility hardly changes upon binding of target peptide. Therefore, the increase in L induced by the binding of peptide suggests a reduction of the linker flexibility.

In order to specify the location of the peptide in the complex, a multibody model depicted in the inset of Fig. 5 was applied. Because the global conformation of apoCaM consists

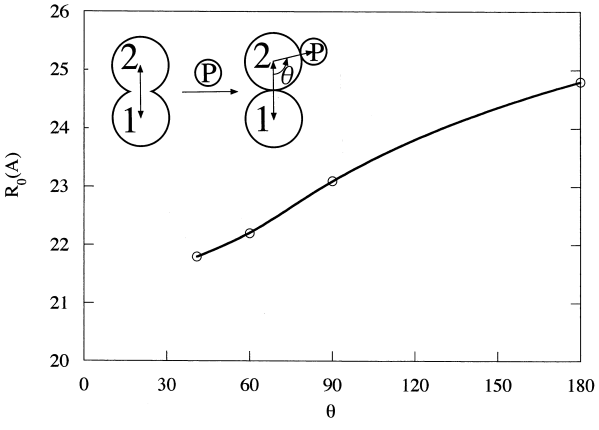

Fig. 5. The rotational angle (θ) dependence of R_0 values calculated for a multibody model shown in the inset, in which 1, 2 and P represent the N- and C-terminal lobes and the peptide, respectively.

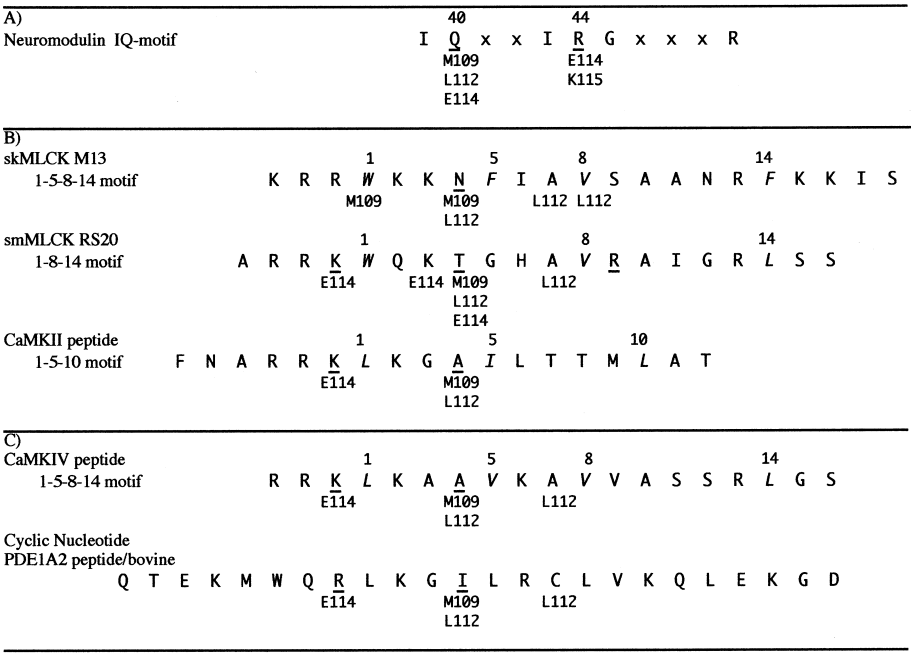

Fig. 6. Residue pairs predicted for apoCaM with a neuromodulin IQ motif (A), residue pairs observed for Ca^{2+}-dependent CaM binding motifs which interact with M109, L112 and E114 of CaM (B), and putative residue pairs for apoCaM with the CaMKIV peptide, suggesting that cyclic nucleotide PDE1A2 peptide also interacts with apoCaM in a similar fashion (C). The underlined residues on Ca^{2+}-dependent CaM binding motifs could play a key role in the interaction with apoCaM.

of two quite separate but compact globular domains, it induces the increase in L upon binding of the peptide. Moreover, we assume that, when bound to apoCaM, the peptide is only partially helical, as suggested by recent studies [21,22]. The radius of gyration of the complex, R_0, making no assumption about shape [43], is:

$$(M_1 + M_2 + M_3)R_0^2 =$$

$$M_1(R_1^2 + L_{G1}^2) + M_2(R_2^2 + L_{G2}^2) + 1pcM_3(R_3^2 + L_{G3}^2)$$

where M_n and R_n are the molecular weight and the radius of gyration of body n, respectively, and L_{Gn} is the center-to-center distance between the complex and the body n. Here $n = 1$, 2 and 3 represent the N- and C-terminal lobes and the peptide, respectively. The location of the peptide can then be defined by a rotational angle around the center of gravity of one lobe, θ. The calculated values of R_0 were plotted as a function of θ in Fig. 5. The experimental value of R_0 for the complex, 22.2 Å, was reproduced, when the peptide locates at $\theta \sim 60°$. Furthermore, the Kratky plots for this model were calculated using the well-known Debye formula [44], in which each body was described by the Guinier approximation [32]. The characteristics in the Kratky plots shown in Fig. 4 were reproduced again, when the peptide locates at $\theta \sim 60°$. These results suggest that the peptide interacts with one lobe of apoCaM at $\theta \sim 60°$, while in order to interact with both lobes of apoCaM, the peptide has to locate at $\theta \sim 41°$.

4.2. ApoCaM/CaMKIV-19 peptide interactions

In order to discuss the interactions between the target peptide and one lobe of apoCaM, we assume that the peptide interacts solely with the C-terminal lobe of apoCaM. The binding of apoCaM to the CaMKIV-19 peptide resembles the only well-characterized apoCaM/peptide interaction, that of the apoCaM/neuromodulin peptide complex [45,46]. It also resembles the interaction of apoCaM/PDE peptide [21] as well as apoCaM/smMLCK RS20 [22,24]. Furthermore, it is thought that in these complexes, the C-terminal lobe of apoCaM bound to the target peptide adopts a semi-open conformation whereas the N-terminal lobe of apoCaM is completely closed [45].

A comparison between the neuromodulin IQ motif and Ca^{2+}-dependent CaM-binding motifs reveals little homology. Fig. 6 shows the putative residue pairs between a target peptide and apoCaM [15–17,21,48]. Here we noted four residues of M109, L112, E114 and K115 of the C-terminal lobe of CaM which interact with Q40 and R44 of the IQ motif [47]. Moreover, these residues of M109, L112, E114 and K115 locate at $\theta \sim 60°$. We searched for the residue pairs on typical Ca^{2+}-dependent CaM-binding motifs which interact with these residues of CaM. Both apoCaM and Ca^{2+}/CaM bind to the same region of these motifs, as suggested by the SAXS analysis and a previous study [48]. We found a common feature at the location of residues on the binding motifs. That is, the residues at 0 and 4, using numbering based on the motifs, have roles in binding with the C-terminal lobe of apoCaM. As M109 and L112 of apoCaM are largely buried inside the lobe [40–42], i.e. the lobe is completely closed, these residues are exposed on the surface of the lobe by the complex formation. For this reason, it is thought that the C-terminal lobe of apoCaM adopts a semi-open conformation in the complex state. The present results suggest that the semi-open conformation does not pre-exist in the C-terminal lobe of apoCaM but is induced by the binding of the target peptide [49,50]. The residues E114 and K115 of apoCaM would interact with the

peptide prior to exposure above hydrophobic residues on its surface because these residues are located on the surface of the C-terminal lobe of apoCaM.

Thus, the decrease in A_2 and B_{if} could be due to the electrostatic and van der Waals interactions between apoCaM and the peptide. It is likely that apoCaM binds to the target peptide, utilizing a binding motif such as the IQ motifs and non-contiguous binding sites [51]. Moreover, it is presumed that smMLCK RS20 and cyclic nucleotide PDE1A2 peptide also interact with apoCaM in a similar manner. However, a complete understanding of the mechanism of apoCaM's interaction with its target peptide awaits determination of the three-dimensional structure of apoCaM complexed with its target peptide.

4.3. Conclusion

The present SAXS results provide strong evidence that apoCaM binds the CaMKIV-19 peptide in the absence of Ca^{2+} and the overall conformation of apoCaM remains unchanged upon binding of the peptide except for the decrease of the flexibility of the central linker. An analysis of residue pairs between CaM and the target peptides suggests that the complex formation is induced by electrostatic interactions and subsequent van der Waals interactions, which correspond to the decrease of A_2 and B_{if}.

Acknowledgements: This work was supported in part by a Grant-in-Aid for Scientific Research from the Ministry of Education, Science, and Culture, Japan (Proposal No. 10450358 to Y.I.). SAXS measurements were performed with the approval of the Photon Factory Advisory Committee, KEK, Tsukuba, Japan (Proposal No. 95G274, 97G131 and 99G350).

References

[1] Eldik, L.J.V. and Watterson, D.M. (1998) Calmodulin and Calcium Signal Transduction, Academic Press, San Diego, CA.
[2] Means, A.R., VanBerkum, M.F.A., Bagchi, I., Lu, K.P. and Rasmussen, C.D. (1991) Pharmacol. Ther. 50, 255–270.
[3] Vogel, H.J. (1994) Biochem. Cell Biol. 72, 357–376.
[4] James, P., Vorherr, T. and Carafoli, E. (1995) Trends Biochem. Sci. 20, 38–42.
[5] Finn, B.E., Evenas, J., Drakenberg, T., Waltho, J.P., Thulin, E. and Forsen, S. (1995) Nat. Struct. Biol. 2, 777–783.
[6] Kretsinger, R.H., Rudnick, S.E. and Weissman, L.J. (1986) J. Inorg. Biochem. 28, 289–302.
[7] Seaton, B.A., Head, J.F., Engelman, D.M. and Richards, F.M. (1985) Biochemistry 24, 6740–6743.
[8] Heidorn, D.B. and Trewhella, J. (1988) Biochemistry 27, 909–915.
[9] Persechini, A. and Kretsinger, R.H. (1988) J. Biol. Chem. 263, 12175–12178.
[10] Barbato, G., Ikura, M., Kay, L.E., Pastor, R.W. and Bax, A. (1992) Biochemistry 31, 5269–5278.
[11] Spoel, D.V.D., De Groot, B.L., Heyward, S., Berendsen, H.J.C. and Vogel, H.J. (1996) Protein Sci. 5, 2044–2053.
[12] Matsushima, N., Izumi, Y., Matsuo, T., Yoshino, H., Ueki, T. and Miyake, Y. (1989) J. Biochem. 105, 883–887.
[13] Heidorn, D.B., Seeger, P.A., Rokop, S.E., Blumenthal, D.K., Means, A.R., Crespi, H. and Trewhella, J. (1989) Biochemistry 28, 6757–6764.
[14] Kataoka, M., Vogel, H.J., Seaton, B.A. and Engelman, D.M. (1989) Proc. Natl. Acad. Sci. USA 86, 6944–6948.
[15] Ikura, M., Clore, G.M., Gronenborn, A.M., Zhu, G., Klee, C.B. and Bax, A. (1992) Science 256, 632–638.
[16] Meador, W.E., Means, A.R. and Quiocho, F.A. (1992) Science 257, 1251–1255.
[17] Meador, W.E., Means, A.R. and Quiocho, F.A. (1993) Science 262, 1718–1721.
[18] Milos, M., Schaer, J.J., Comte, M. and Cox, J.A. (1988) J. Biol. Chem. 263, 9218–9222.
[19] Izumi, Y., Yoshino, H., Matsuo, T., Matsushima, N., Ueki, T., Kobayashi, K. and Miyake, Y. (1988) Rep. Prog. Polym. Phys. Jpn. 31, 571–574.
[20] Yoshino, H., Minari, O., Matsushima, N., Ueki, T., Miyake, Y., Matsuo, T. and Izumi, Y. (1989) J. Biol. Chem. 264, 19706–19709.
[21] Yuan, T., Walsh, M.P., Sutherland, C., Fabian, H. and Vogel, H.J. (1999) Biochemistry 38, 1446–1455.
[22] Tsvektov, P.O., Protaesvich, I.I., Gilli, R., Lafitte, D., Lobachov, V.M., Haiech, J., Briand, C. and Makarov, A. (1999) J. Biol. Chem. 274, 18161–18164.
[23] Urbauer, J.L., Short, J.H., Dow, L.K. and Wand, A.J. (1995) Biochemistry 34, 8099–8109.
[24] Hill, T.J., Lafitte, D., Wallace, J.I., Cooper, H.J., Tsvektov, P.O. and Derrick, P.J. (2000) Biochemistry 39, 7284–7290.
[25] Mosialos, G., Hanissian, S.H., Jawahar, S., Vara, L., Kieff, E. and Chatila, T.A. (1994) J. Virol. 68, 1697–1705.
[26] Kitani, T., Okuno, S. and Fujisawa, H. (1994) J. Biochem. 115, 637–640.
[27] Bland, M.M., Monroe, R.S. and Ohmstede, C.A. (1994) Gene 142, 191–197.
[28] Rhoads, A.R. and Friedberg, F. (1997) FASEB J. 11, 331–340.
[29] Yoshino, H., Wakita, M. and Izumi, Y. (1993) J. Biol. Chem. 268, 12123–12128.
[30] Lowry, O.H., Rosebrough, N.J., Farr, A.L. and Randall, R.J. (1951) J. Biol. Chem. 193, 265–275.
[31] Ueki, T., Hiragi, Y., Kataoka, M., Inoko, Y., Amemiya, Y., Izumi, Y., Tagawa, H. and Muroga, Y. (1985) Biophys. Chem. 23, 115–124.
[32] Guinier, A. and Fournet, G. (1955) Small-Angle Scattering of X-Rays, pp. 126–133, Wiley, New York.
[33] Izumi, Y., Wakita, M., Yoshino, H. and Matsushima, N. (1992) Biochemistry 31, 12266–12271.
[34] Kratky, O. and Porod, G. (1949) Rec. Trav. Chim. Pay-Bas 68, 1106–1122.
[35] Kratky, O. (1966) in: Small-Angle X-Ray Scattering (Brumberger, H., Ed.), pp. 63–120, Gordon and Breach, New York.
[36] Kratky, O. (1982) in: Small Angle X-ray Scattering (Glatter, O. and Kratky, O., Eds.), pp. 361–386, Academic Press, London.
[37] Feigin, L.A. and Svergun, D.I. (1987) Structure Analysis by Small-Angle X-ray and Neutron Scattering, Plenum Press, New York.
[38] Kataoka, M., Flanagan, J.M., Tokunaga, F. and Engelman, D.M. (1994) in: Synchrotron Radiation in the Biosciences (Chance, B., Deisenhofer, J., Ebashi, S. et al., Eds.), pp. 187–194, Clarendon Press, Oxford.
[39] Anderegg, J.W., Beeman, W.W., Shulman, S. and Kaesberg, P. (1955) J. Am. Chem. Soc. 77, 2927–2937.
[40] Zhang, M., Tanaka, T. and Ikura, M. (1995) Nat. Struct. Biol. 2, 758–767.
[41] Kuboniwa, H., Tjandra, N., Grzesiek, S., Ren, H., Klee, C. and Bax, A. (1995) Nat. Struct. Biol. 2, 768–776.
[42] Finn, B.E., Evenas, J., Drakenberg, T., Waltho, J.P., Thulin, E. and Forsen, S. (1995) Nat. Struct. Biol. 2, 777–783.
[43] Goldstein (1962) in: Classical Mechanics, pp. 149–151, Addison-Wesley, Reading, MA.
[44] Debye, P. (1915) Ann. Phys. 46, 809–823.
[45] Houdusse, A. and Cohen, C. (1995) Proc. Natl. Acad. Sci. USA 92, 10644–10647.
[46] Houdusse, A., Silver, M. and Cohen, C. (1996) Structure 4 (12), 1475–1490.
[47] Swindells, M.B. and Ikura, M. (1996) Nat. Struct. Biol. 3 (6), 501–504.
[48] Moore, C.P., Rodney, G., Zhang, J.Z., Santacruz-Toloza, L., Strasburg, G. and Hamilton, S.L. (1999) Biochemistry 38 (26), 8532–8537.
[49] Nelson, M.R. and Chazin, W.J. (1998) Protein Sci. 7, 270–282.
[50] Nelson, M.R. and Chazin, W.J. (1998) BioMetals 11, 297–318.
[51] Jurado, L.A., Chockalingam, P.S. and Jarrett, H.W. (1999) Physiol. Rev. 79 (3), 661–682.
[52] Izumi, Y., Matsushima, N. and Yoshino, H. (1989) J. Jpn. Soc. Synchrotron Rad. Res. 2 (1), 23–33.